VARIATION IN STRUCTURAL FEATURES INDUCED BY ORTHO-SUBSTITUTED BENZOATE LIGAND IN ZINC CYCLAM-BASED COMPOUND: SYNTHESIS, CHARACTERIZATION AND HIRSCHFELD STUDIES

Nikita Harmalkar[a], Sunder N. Dhuri[a]*

[a]*School of Chemical Sciences, Goa University, Taleigao Plateau, Goa, 403 206 India,*

Corresponding author: sndhuri@unigoa.ac.in

Abstract

The variability of carboxylate linkers in eight new $[Zn(II)(cyclam)]^{2+}$ compounds (**1**-**8**) leading to rich structural diversity and dimensionality is presented in this paper. The $[Zn(II)(cyclam)]^{2+}$ featuring *ortho*-substituted benzoate ligands were synthesized and characterized by various tools. Compounds **1** and **2** exhibit one-dimensional polymeric structures, wherein aqua ligands bridging cationic and anionic units leading to $[Zn_2(\mu\text{-}H_2O)_2(cyclam)(L)_4]$ (where L = = *o*-methyl benzoate in **1**, L = *o*-methoxy benzoate in **2**, cyclam = 1,4,8,11-tetraazacyclotradecane). Hydroxy and nitro substitution at *ortho* positions have led to zero-dimensionality in compounds **3** and **4**, $[Zn(C_{10}H_{24}N_4)(L)_2]$ (L = *o*-hydroxybenzoate in **3**, L = *o*-nitrobenzoate in **4**). Interestingly, using benzoate, o-chlorobenzoate, *o*-(methylthio)benzoate, and *o*-aminobenzoate substituents resulted in significant variation in the crystal packing, leading to discrete ionic compounds **5**-**8**. An investigation into isostructurality revealed a higher cell similarity and a lower isostructurality index for the **1**,**2** pair; in contrast, the pair of **3**,**4** and a group of compounds **5**-**7** were identified as non-isostructural. To get a deeper insight into the noncovalent interactions governing the supramolecular self-assemblies, we have performed Hirshfeld surface analysis for all compounds, and the results are presented.

Keywords: Zinc cyclam crystal structures, Isostructurality, Hirshfeld analysis, supramolecular, carboxylate interaction.

1. Introduction

Cyclam (1,4,8,11-tetraazacyclotetradecane) is a macrocyclic N-donor ligand that has been generously employed in the synthesis of metal complexes due to its ability to render inertness and chemical stability to the metal complex in its parent form or when is suitably *N*-functionalized [1-2]. The metal chelates prepared using cyclam find their application in various fields, including medicine, catalysis, and molecular sensors[3-6]. Besides offering high binding affinity to small transition metal ions, cyclam also adopts various configurations due to its flexibility when interacting with the metal ions and the other supporting ligands. In 1965, Bosnich *et al*. described five configurations adopted by the cyclam ligand under the influence of the transition metal ion [7]. The orientation of the N-H group in coordinated cyclam defines the type of isomer, which can be classified as *trans*-I- IV, and the unusual folded *cis*-V configuration in the metal compounds. Among these, the *trans*-III configuration is the most stable and predominates in the cyclam-based compounds compared to the other forms[8-11]. The nature of the counter anion greatly influences the relative population of the different configurations present in the solution state [12,13]. In 2003, Sadler *et al*., *via* the NMR technique, highlighted the influence of the counterion on the type of isomer present in the solution state. In addition, the solid-state examination of the crystal structure provided valuable information on the configuration adopted by the cyclam ligand.

The structural insights into the chelating metal complexes, such as those involving cyclam ligands, play a crucial role in understanding their properties and potential applications, such as inhibitory effect on the replication of human immunodeficiency virus (HIV). In the case of cyclam-based compounds, the interaction with the co-receptor CXCR4 is indeed intriguing. The carboxylate group of the aspartate residue in CXCR4 likely forms non-covalent interactions with the cyclam ligand, contributing to its binding affinity[14,15]. Given these, developing new anti-HIV drugs of cyclam compounds requires a better understanding of the conformations and crystal packing forces. Due to the tendency of the cyclam ligand to adopt different configurations, the coordinated cyclam may be recognized by the receptor differently. This has invoked an increasing activity in studying the interaction of the carboxylate moieties with metal cyclam core. In 2005, Jo *et al*, studied the molecular interaction of four compounds $[Zn(L)(tp)]\cdot H_2O$, $[Zn(L)(H_2bta)]\cdot 2H_2O$, $[Zn_2(L)_2(ox)]_2ClO_4\cdot 2DMF$ and $[Zn(L)(H_2bta)]\cdot 2H_2O$ where L = cyclam, tp = 1,4-benzenedicarboxylate, H_2bta = 1,2,4,5-benzenetetracarboxylate, ox = oxalate and H_2btc = 1,3,5-

benzenetricarboxylate ions. The structural analysis of the above compounds reveals strong coordination of the carboxylate anions with the $[Zn(cyclam)]^{2+}$ core. The presence of the oxalate ligand, which adopts a bridging coordination mode, in compound $[Zn_2(L)_2(ox)]_2ClO4 \cdot 2DMF$, thereby forcing the cyclam ligands on each zinc ion to adopt the *cis*-V configuration. Meanwhile, the cyclam in the other mononuclear compounds adopts the most stable *trans*-III configuration around the zinc ion [16]. In 2006, Kim *et al* studied the molecular interaction of two metal cyclam compounds, namely $[Zn(L)(Maleate)] \cdot H_2O$, $[Zn(L)(H_2O)_2](fumarate) \cdot 4H_2O$ where L = cyclam. Incorporating a dibasic maleate ligand formed a 1D coordination polymer wherein the maleate ligand bridges the two $[Zn(cyclam)]^{2+}$ cores and forms a coordinatively saturated compound. On the contrary, the fumarate ligand, having a similar basicity as that of maleate, does not coordinate with the central metal ion. This selective, strong interaction with zinc was assumed to be because of the conformation of the ligand, which enables the formation of hydrogen bonds as compared to the fumarate ligand, where the carboxylate groups are trans to each other [17]. As the example above shows, the crystal packing arrangements can be altered by changing the chemical composition, which can also be achieved by modifying the substituents. Their type and placement in a multi-component system can gradually influence the crystal packing arrangement, potentially leading to the formation of isostructural compounds or disruption in isostructurality. For related compounds to exhibit isostructurality, they must share a similar chemical composition and conformation of the compounds, with the highly analogous supramolecular arrangement in the crystal lattice having the same space group.[18-20] Bombicz and co-workers highlighted various methods to recognize isostructurality in related compounds. These methods include numerical descriptors such as cell similarity (π), isostructurality (*Is*), and molecular isometricity indices. Statistical approaches help investigate the extent of isostructurality exhibited by related compounds with the same space group and Z[18]. Our work intends to expand the literature on zinc-cyclam-based compounds with varying *ortho* substituents and further extend our understanding of the mode of interaction of the carboxylate anions with the zinc-cyclam unit and their influence on the supramolecular arrangement.

2. Results and discussion

2. 1. Synthetic aspects, spectroscopic and structural characterization of 1-8

The crystallographic data and the refinement parameters of compounds **1**-**4** are given in **Table 1**, and **5**-**8** are given in **Table S1**. Compounds **1**-**8** were obtained *via* slow evaporation method at room temperature, wherein aqueous $Zn(OAc)_2 \cdot 2H_2O$ solution was initially mixed with the corresponding carboxylic acid (L1-L8) separately and stirred at 80°C until a clear solution was obtained. The resulting solution was then reacted with cyclam ligand for 1 hr. Upon standing at room temperature, this reaction mixture afforded suitable single crystals of compounds **1**-**8**, which were then washed using cold distilled water and used for further analysis. A general scheme showing the synthetic route for **1**-**8** is shown in **Scheme 1**. The IR spectroscopic analysis revealed that compounds exhibit sharp bands in the region of ~1700 and 1400 cm^{-1}, which are attributed to the characteristic absorption band for asymmetric and symmetric stretching vibration of the carboxylate (COO^-) anion, thus suggesting the incorporation of the carboxylate moieties in the respective compounds as depicted in **Figure S1**. The broad absorption band centered at 3369 (**1**), 3398 (**2**), 3310(**3**), 3340(**4**), 3412(**5**), and 3378 (**6**) cm^{-1} is attributed to the O-H stretching vibration of the aqua molecules. Medium to weak stretching vibration bands due to C-H and N-H vibration in the organic moieties were seen in the 3100 -2800 cm^{-1} range in all eight compounds.

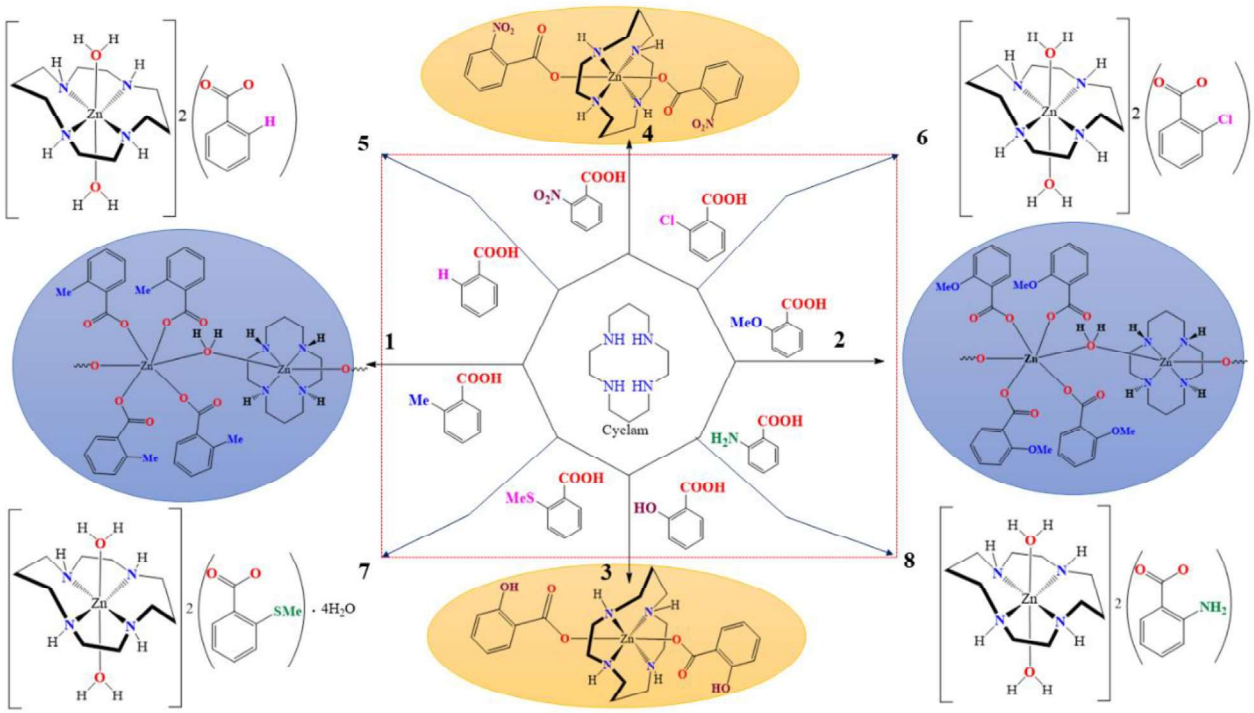

Scheme 1. General preparative scheme for compounds **1-8**

2.2. Thermal investigation of compounds 1 and 5

The thermal decomposition pattern of compound **1** was compared with the decomposition pattern of **5**, consisting of the parent benzoate ligand. The thermal profiles of **1** are depicted in **Figure 1**. The first mass loss in both compounds is due to the removal of the coordinated water molecules. In compound **1,** the first mass loss occurs between 90-150ºC, accounting for 4 % (*calcd.* 3.97 %) mass loss attributed to the loss of the bridging type of aqua molecules with two endotherms in the DTA pattern centered at 118 and 145 ºC. In contrast, in compound **5** (**Figure S2**), the aqua molecules are lost at a much lower temperature range, between 80 °C to 125 °C, due to the monodentate coordination mode of the water molecules. This process is evident from an endotherm at 87 °C in the DTA pattern. The following mass loss of 22.72 % (*calcd*. 22.07 % in **1**) and 36.92 % (*calcd*. 37 % in **5**) is attributed to the decomposition of the cyclam ligand in the range of 250 -350°C. Upon dehydration and decomposition of the cyclic amine, further heating in **1** till 700 °C results in a mass loss of 56.17 % in **1** (*calcd*. 56.05 %) and 39.28 % in **5** (*calcd*. 41.6 %) is observed due to the decomposition of the carboxylate ligands, (*o*-methoxybenzoate and benzoate) in respective compounds. The final residue of 17.22 % was observed in the case of compound **1**

and is in good agreement with the calculated 17.9 % for ZnO. Similar results were obtained for compound **5**.

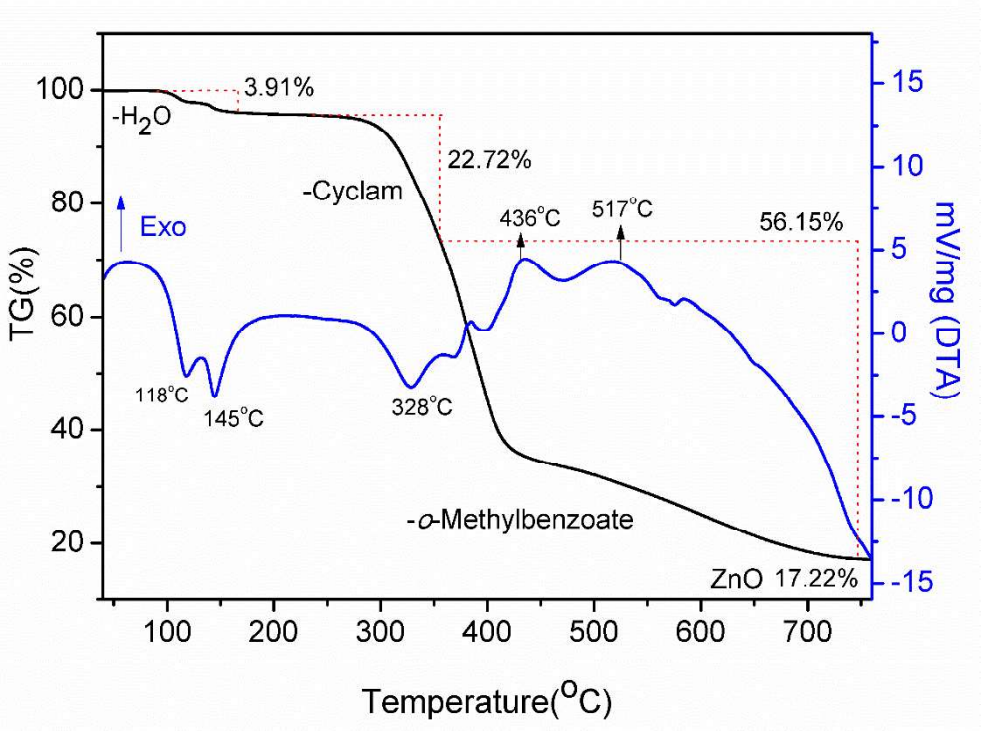

Figure 1. The thermal decomposition plot of compound **1** was recorded in the nitrogen atmosphere between room temperature to 760 °C at a heating rate of 10 °C min^{-1}.

2.3. Structural description of crystal structure, isostructurality descriptors, and Hirshfeld analysis 1-8

The structural analysis of the eight compounds reveals that the macrocyclic ligand consistently adopts the *Trans*-III configuration irrespective of the carboxylate anion used, which is recognized as the most stable configuration adopted by the cyclam ligand. The observed structural variation is thus primarily attributed to the interactions between the carboxylate anions with varying *ortho* substituents and the zinc cyclam core. Moreover, the compounds were classified based on the similarities in their unit cell parameters and examined for isostructurality. For a compound to demonstrate isostructurality, it must have unit cell parameters similar to those of related compounds. The zinc series, consisting of eight compounds, was divided into three groups to elucidate the structural relationship and variation among them. Compounds **1** and **2** were placed in *Group I* as they crystallized in the monoclinic system with the *C*2/*m* space group. **3** and **4** were

assigned to *Group II* as they crystallized in the orthorhombic system with *P b c a* space group. *Group III* included compounds **5**, **6**, and **7** crystallized in the monoclinic $P2_1/n$ space group. Compound **8** did not fit into these groups, as it crystallized in the monoclinic crystal system with the *C*2/*c* space group.

The crystal structure of compounds **1** and **2** (*Group I*) exhibits a one-dimensional *zig-zag* chain structure due to bridging aqua molecules located on a two-fold crystallographic axis that binds to the $[Zn(cyclam)]^{2+}$ cationic and the anionic units $[Zn(L)_4]^{2-}$. The crystal structure of compound **1**, shown in **Figure 2a**, comprises two crystallographically independent Zn^{2+} ions occupying the special positions (Zn1 and Zn2) and adopts distorted octahedral geometry. The Zn···Zn distance across the chain is 4.318 Å. The Zn1 ion is coordinated with the cyclam ligand *via* four nitrogen atoms (N1, N1i, N1ii, N1iii) on the equatorial plane. The axial positions are occupied by the oxygen atom (O1W and $O1W^{iii}$) from the bridging aqua molecules, thus forming {ZnN4O2} coordination environment. On the other hand, the Zn^{2+} ion is coordinated to six oxygen atoms forming the {ZnO6} core, wherein the four oxygen atoms are contributed by the carboxylate group of *o*-methyl benzoate ligands (L) as depicted in **Figure 2b**. The O-donor ligand adopts a monodentate coordination mode, and axial oxygen atoms are contributed by the bridging aqua molecules (O1W and $O1W^{iii}$). A similar crystal structural arrangement is identified in compound **2,** shown in the ORTEP diagram **Figure S3**.

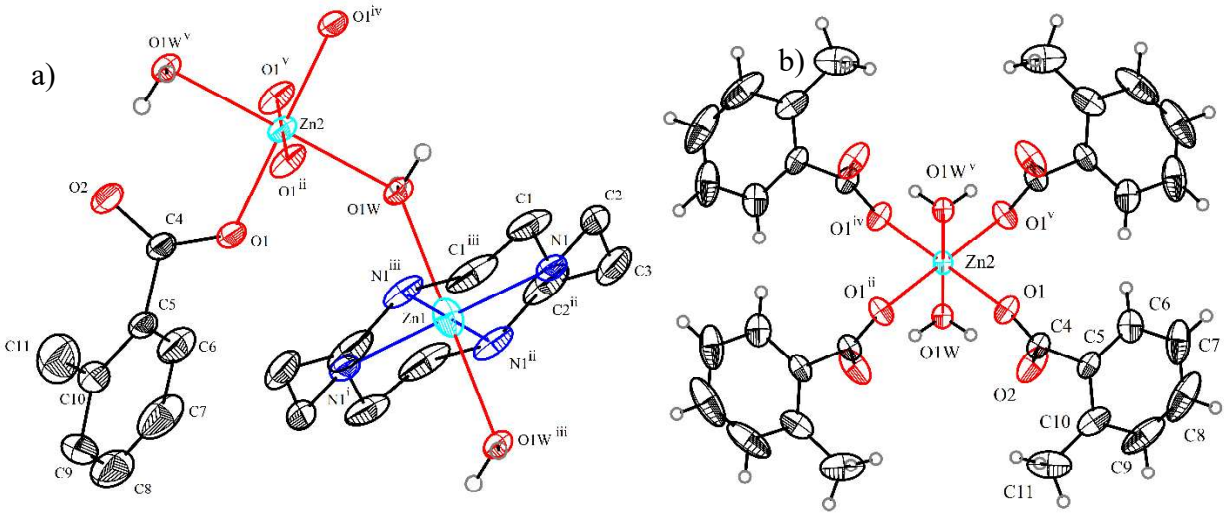

Figure 2 a) The ORTEP diagram of compound **1** shows a portion of the chain with an atom labeling scheme. Thermal ellipsoids are drawn at 30 % probability except for the hydrogen atoms.

The hydrogen atoms on the cyclam and the carboxylate ligand have been omitted for clarity. Symmetry codes *i) -x, 1-y, 1-z, ii) x, 1-y, z, iii) -x, y, 1-z, iv) 1-x, 1-y, 1-z and v) 1-x, y, 1-z* b) Carboxylate adopting monodentate coordination mode around Zn2 ion in compound **1**.

The Zn1 and Zn2 atoms in both compounds show distorted octahedrons due to the elongation of the axial bonds. For instance, the O1W atom coordinated to the $[Zn(cyclam)]^{2+}$ unit shows a longer Zn1-O1W bond distance of 2.448(17) and 2.463(4) Å as compared to the O1W atom coordinated to the $[Zn(L)_4]^{2-}$ unit with the bond distance of 2.255(17) and 2.222(3) Å in **1** and **2** respectively. Even though the acid counterpart is different, the Zn1-O1W-Zn2 bond angles in both compounds are very close, at **1** 133.23 (19) and **2** 132.49 (17)°. The selected bond distances and angles for **1** and **2** are summarized in **Table 2**. Similar distortion is seen in related aqua-bridged compounds reported in the literature[21-25].

A better view of the non-covalent inter-molecular hydrogen bonding interactions such as N-H···O, O-H···O, and C-H···O, along with π-π stacking interactions between aromatic benzene rings of the acid component aid in stabilizing the crystal lattice are achieved with structural analysis. Each cationic unit interacts with an anionic unit with the help of $N1\text{-}H1_{(cyclam)}\cdots O1_{(carboxylate)}$ with a donor-acceptor distance of 3.012 Å. Further, the hydrogen atoms of the bridging aqua ligand are also involved in hydrogen bonding with the uncoordinated oxygen atoms of the carboxylate ligand $O1W\text{-}H1W_{(aqua)}\cdots O2_{(carboxylate)}$ with a donor-acceptor distance of 2.62 Å, thus playing significant in the stabilization of the structure. The formation of a one-dimensional (1-D) coordination polymer with intermolecular hydrogen bonds is shown in **Figure 3a**. Moreover, the 1-D chain is also supported through C-H···O and π-π interactions. Each adjacent aromatic ring of the carboxylate interacts with weak π-π stacking interaction (centroid distance of 4.82 Å), as shown in **Figure 3b**. These weaker interactions extend the 1-D chain into a 3-D supramolecular network and stabilize the crystal structure.

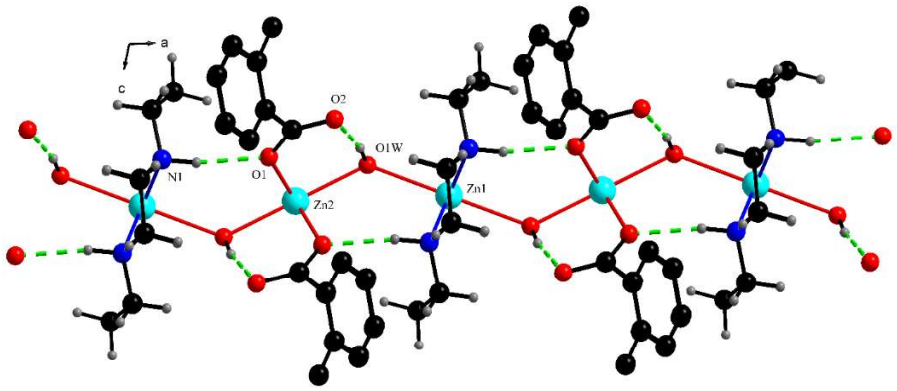

Figure 3a. 1-D chain structure due to bridging aqua molecules running along '***a***' axis. Green dotted lines show the intermolecular hydrogen bonds.

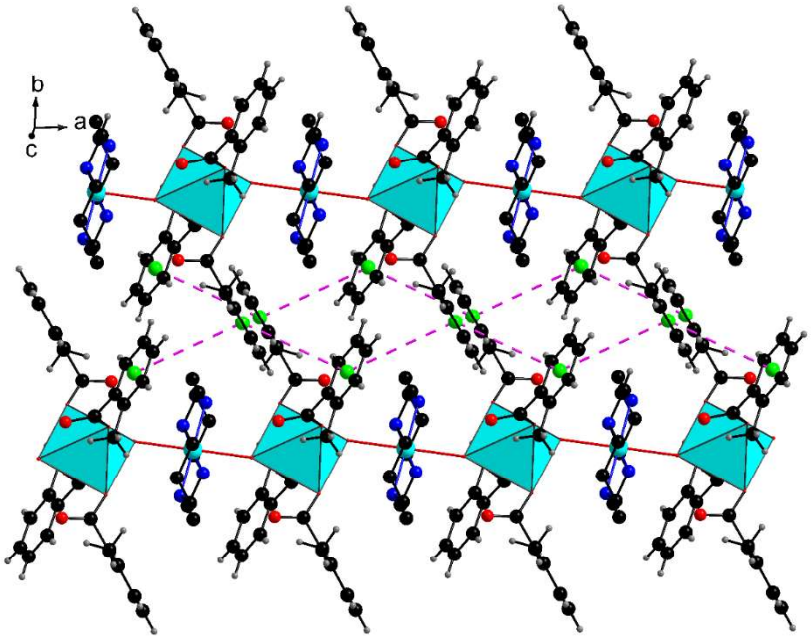

Figure 3b. The weak π-π interactions between the aromatic rings of the adjacent chains with a centroid distance of 4.82 Å

Table 1. The crystallographic data and structure refinement parameters for **1-4**.

Absorption correction: Semi-empirical from equivalents. Refinement method: Full-matrix least-squares on F^2.

Compound	**1**	**2**	**3**	**4**
Empirical formula	$C_{42}H_{56}N_4O_{10}Zn_2$	$C_{42}H_{56}N_4O_{14}Zn_2$	$C_{24}H_{34}N_4O_6Zn$	$C_{24}H_{32}N6O_8Zn$
Formula Weight (g)	907.68	971.68	539.94	597.95
Temperature (K)	296 (2)	296 (2)	296 (2)	296 (2)
Wavelength (Å)	0.71073	0.71073	0.71073	0.71073
Crystal system	Monoclinic	Monoclinic	Orthorhombic	Orthorhombic
Space group	*C* 2/*m*	*C* 2/*m*	*Pbca*	*Pbca*
Unit cell dimensions (Å/°)	a= 8.6359(7) b = 22.2604(16) c = 11.6583(9) β= 103.563(3)	a= 8.5789(8) b = 22.352(2) c = 11.6195(10) β= 97.157(3)	a= 13.2057(6) b = 10.6115(5) c = 17.6741(8) β= 90	a= 13.3732(5) b = 11.096(4) c = 17.8362(7) β= 90
Volume ($Å^3$)	2178.7(3)	2210.8(3)	2476.7(2)	2646.70(17)
Z	4	4	4	4
Density (calcd.) (Mg/m^3)	1.384	1.46	1.448	1.501
Absorption coefficient (mm^{-1})	1.16	1.155	1.039	0.987
F(000)	952	1016	1136	1248
Crystal size (mm^3)	0.30x 0.11 x 0.09	0.31x 0.25 x 0.15	0.42x 0.31 x 0.15	0.43x 0.27 x 0.12
θ range (°)	2.593 to 28.325	2.538 to 28.358	2.719 to 28.294	2.745 to 28.284
Index ranges	-11≤h≤11, -29≤k≤29, -15≤l≤15	-11≤h≤11, -29≤k≤29, -15≤l≤15	-17≤h≤17, -14≤k≤14, -23≤l≤23	-17≤h≤17, -14≤k≤14, -23≤l≤23
Reflections collected	32271	25506	69830	85827
Independent reflections	2781 [R(int) = 0.0335]	2830 [R(int) = 0.0713]	3078[R(int) = 0.0547]	3279 [R(int) = 0.0379]
Completeness to theta = 25.242° (%)	99.8	99.9	100	99.8
Data/restraints/parameters	2781 / 0 / 142	2830 / 0 / 156	3078 / 0 / 172	3279 / 0 / 186
Goodness-of-fit on F^2	1.018	1.149	1.15	1.075
Final R indices [I>2sigma(I)]	R1 = 0.0335, wR2 = 0.0836	R1 = 0.0577, wR2 = 0.1478	R1 = 0.0343, wR2 = 0.0847	R1 = 0.0315, wR2 = 0.0805
R indices (all data)	R1 = 0.0437, wR2 = 0.0896	R1 = 0.0799, wR2 = 0.1626	R1 = 0.0604, wR2 = 0.1126	R1 = 0.0407, wR2 = 0.0919
Extinction coefficient	n/a	n/a	n/a	n/a
Largest diff. peak and hole ($e.Å^{-3}$)	0.266 and -0.888	0.788 and -1.045	0.294 and -0.524	0.472 and -0.405
CCDC No	2376524	2376525	2376526	2376527

Table 2. Selected hydrogen bond distance and bond angles for **1** and **2**.

1					
Bond distance		*Bond angle*			
Zn1-N1	2.0777(17)	N1-Zn1-O1W	91.89(5)	O1W-Zn2-O1	86.41(5)
Zn1-N1^{i}	2.0778(17)	N1^{ii}-Zn1-O1W	88.1(5)	O1W-Zn2-O1^{ii}	86.41(5)
Zn1-N^{ii}	2.0778(17)	N1^{i}-Zn1-O1W	91.9(5)	O1W-Zn2-O1^{iv}	93.59(5)
Zn1-N^{iii}	2.0778(17)	N1^{iii}-Zn1-O1W	91.9(5)	O1W-Zn2-O1^{v}	93.59(5)
Zn1-O1W^{iii}	2.4484(17)	N1-Zn1-N1^{ii}	94.34(12)	O1-Zn2-O1^{ii}	91.73(9)
Zn1-O1W	2.4484(17)	N1^{i}-Zn1-N1^{ii}	85.66(12)	O1^{ii}-Zn2-O1^{iv}	88.27(9)
Zn2-O1^{iv}	2.0564(13)	N1^{i}-Zn1-N1^{iii}	94.34(12)	O1^{iv}-Zn2-O1^{v}	91.73(9)
Zn2-O1^{ii}	2.0564(13)	N1-Zn1-N1^{iii}	85.66(12)	O1^{v}-Zn2-O1	88.27(9)
Zn2-O1^{v}	2.0564(13)	N1^{iii}-Zn1-N1^{ii}	180(7)	O1W-Zn2-O1W^{v}	180
Zn2-O1	2.0564(13)	N1^{i}-Zn1-N1	180(7)	O1-Zn2-O1^{iv}	180
Zn2-O1W	2.2553(17)	O1W-Zn1-O1W^{iii}	180(7)	O1^{ii}-Zn2-O1^{v}	180
Zn2-O1W^{v}	2.2553(17)				
2					
Bond distance		*Bond angle*			
Zn1-N1	2.074(3)	N1-Zn1-O1W	91.53(11)	O1W-Zn2-O1	86.99(1)
Zn1-N1^{i}	2.074(3)	N1^{ii}-Zn1-O1W	91.53(11)	O1W-Zn2-O1^{ii}	86.99(1)
Zn1-N^{ii}	2.074(3)	N1^{i}-Zn1-O1W	88.47(11)	O1W-Zn2-O1^{iv}	93.01(1)
Zn1-N^{iii}	2.074(3)	N1^{iii}-Zn1-O1W	88.47(11)	O1W-Zn2-O1^{v}	93.01(1)
Zn1-O1W^{iii}	2.463(4)	N1-Zn1-N1^{ii}	94.4(3)	O1-Zn2-O1^{ii}	91.12(18)
Zn1-O1W	2.463(4)	N1^{i}-Zn1-N1^{ii}	85.6(3)	O1^{ii}-Zn2-O1^{iv}	88.88(18)
Zn2-O1^{iv}	2.065(3)	N1^{i}-Zn1-N1^{iii}	94.4(3)	O1^{iv}-Zn2-O1^{v}	91.12(18)
Zn2-O1^{ii}	2.065(3)	N1-Zn1-N1^{iii}	85.6(3)	O1^{v}-Zn2-O1	88.88(18)
Zn2-O1^{v}	2.065(3)	N1^{iii}-Zn1-N1^{ii}	180(15)	O1W-Zn2-O1W^{v}	180
Zn2-O1	2.065(3)	N1^{i}-Zn1-N1	180	O1-Zn2-O1^{iv}	180
Zn2-O1W	2.222(3)	O1W-Zn1-O1W^{iii}	180	O1^{ii}-Zn2-O1^{v}	180

*Symmtery code (**1**): i= -x, 1-y, 1-z, ii = x, 1-y, z, iii = -x, y, 1-z, iv = 1-x,1-y, 1-z, v = 1-x, y, 1-z, (**2**) i = 2-x, 1-y, 1-z, ii = x, 1-y, z, iii = 2-x, y, 1-z, iv = 1-x,1-y, 1-z, v = 1-x, y, 1-z*

Table 3. Selected hydrogen bond parameters for **1**-**8**

D-H···A	d(D-H)	d(H···A)	<DHA	d(D···A)	Symmetry code
1					
O1-H1W···O2	0.83	1.8	169.17	2.62	1-x, 1-y, 1-z
N1-H1···O1	0.98	2.052	165.8	3.012	-x, 1-y, 1-z
C1-H1A···O2	0.97	2.594	158.56	3.515	1-x, 1-y, 1-z
2					
O1W-H1W···O2	0.804	1.852	165.46	2.638	1-x, y, 1-z
N1-H1···O1	0.764	2.235	170.99	2.992	2-x, 1-y, 1-z
C1-H1A···O2	0.97	2.545	159.48	3.47	1-x, 1-y, 1-z
3					
O3-H1···O2	0.92	1.661	154.67	2.523	
N2-H2···O2	0.834	2.153	162.57	2.959	1-x, 1-y, 1-z
C9-H9A···O2	0.97	2.531	139	3.325	1/2-x, 1/2-y, 1-z
4					
N1-H1···O2	0.852	2.498	141.79	3.211	
C4-H4A···O1	0.97	2.608	113.82	3.129	
C1-H1A···O1	0.97	2.543	116.35	3.098	1-x, 1-y, 1-z
5					
O1W-H1W···O1	0.796	1.887	176.47	2.682	
O1W-H2W···O2	0.765	1.98	159.77	2.711	1-x, 1-y, 1-z
N1-H1···O2	0.98	1.972	169.18	2.94	1-x, y, z
6					
O1W-H1W···O2	0.77	1.892	171.29	2.656	
O1W-H2W···O1	0.795	1.921	157.34	2.673	1-x, 1-y, 1-z
N1-H1···O1	0.98	1.946	168.94	2.914	1+x, y, z
7					
O3W-H1E···O2	0.757	2.131	169.93	2.879	
O3W-H2E···O2W	0.821	2.006	174.46	2.825	
O1W-H2C···O2	0.822	1.923	175.52	2.744	
O1W-H1C···O1	0.829	1.964	169.46	2.783	1-x, 1-y, 1-z
O2W-H1D···O1	0.833	2.037	169.27	2.859	1-x, 1-y, 1-z
8					
N3-H3···O1	0.86	2.075	128.36	2.695	
O1W-H1W···O1	0.707	2.097	173.68	2.801	
O1W-H2W···O1	0.691	2.175	159.74	2.833	x+3/2, 1/2-y, 1-z
O1W-H2W···O2	0.691	2.611	147.49	3.215	x+3/2, 1/2-y, 1-z
N3-H3A···O2	0.86	2.041	167.39	2.887	x, 1-y, 1/2-z

The extent of isostructurality in molecular pairs can be described based on geometrical descriptors such as cell similarity (π), isostructurality (I_s), and molecular isometricity indices. The isostructurality index offers a strict criterion for structural similarity, accounting for the

geometrical and positional differences caused by rotation and translation[18,26]. The cell similarity index obtained for the molecular pair **1** and **2** was 0.037, close to zero, suggesting similar unit cell parameters. However, the lower isostructurality index of 37% indicates a considerable difference in the close packing of the two compounds. Furthermore, the mercury software was used to overlay the asymmetric unit of the related molecules, as depicted in **Figure 4a**, to obtain the rmsD and max D values. A higher deviation of the max D (3.7119 Å) from zero can be attributed to varying orientations of the substituents, which assume almost opposite directions. Analysis of the geometrical parameters of the carboxylate anion highlights how substituents disrupt the isostructurality in compounds **1** and **2**. Due to the ortho effect, the carboxylate group exhibits a slight bend around the ring in both compounds. The dihedral angles between the ring carrying the substituent and the plane defined by (O1-C4-O2) are 64.93 in (**1**), as shown in **Figure 4b**, and 73.82° in compound **2**. Additionally, the torsion angle (C5-C6-C7-C8-C9-C10) in compound **1** is 115.73° and -106.81 in compound **2**. These variations suggest that substituents might greatly induce conformational changes, leading to a loss of isostructurality between the related compounds.

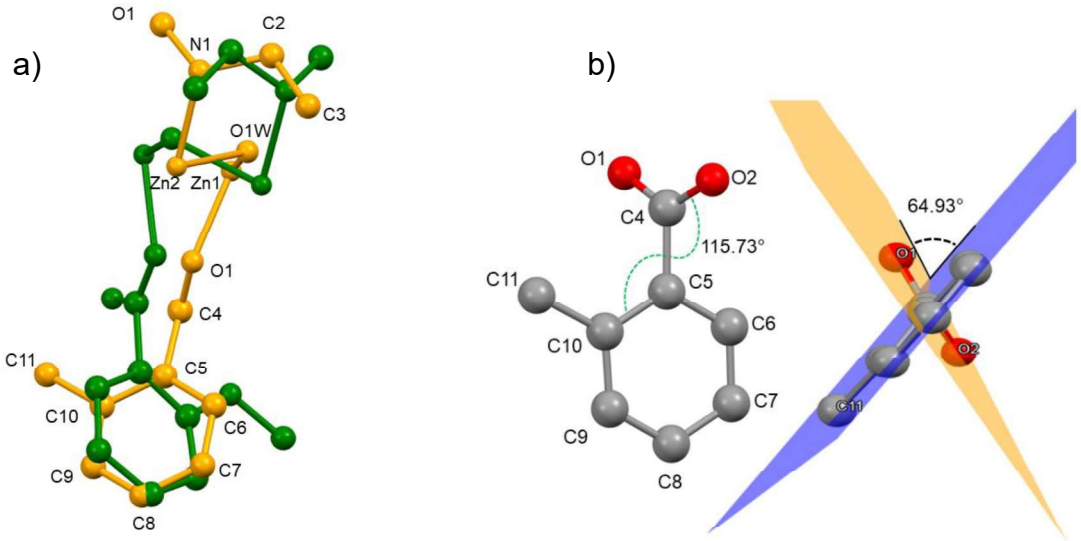

Figure 4 a). Overlay diagram of the asymmetric units of **1** (yellow) and **2** (green) compounds with rmsD = 1.9347 and max = 3.711 Å. **b)**. View along the carboxylate anion highlighting the orientation of the substituents (left) and dihedral angle between the mean plane through benzene ring (C5-C6-C7-C8-C9-C10) and (O1-C4-O2) (right)

To further investigate the supramolecular non-covalent interactions in compounds **1** and **2**, Hirshfeld surface (HS) analysis was performed. HS effectively quantifies the intermolecular interaction in the crystals. The d_{norm} surfaces with short contacts, where the distance between the atoms is shorter than the sum of their van der Waals radii are indicated in red. The d_{norm} mapping reveals strong hydrogen bonds such as N-H···O contacts between the N atoms of the cyclam in the cationic unit and oxygen of the neighboring carboxylate ligand as a bright red area in the surface as shown in **Figure 5a, e** for compounds **1** and **2** respectively. In both compounds, the predominant interactions are of the H···H type, accounting for up to 67 % in compound **1,** which consists of methyl benzoate anion as the anion. However, with the introduction of methoxy benzoate in the structure of compound **2**, the H···H type interaction reduces by 9.4 %. Other significant interactions include C···H/ H···C and O···H/ H···O type seen in both the compounds. Given the change as mentioned earlier in the anion source, an increment of 10% is observed in the contribution from the O···H/ H···O type of interaction in compound **2,** with compound **1** accounting for 12.2%. The intermolecular interactions arising due to C···H/ H···C are nearly the same in both compounds, contributing 19.4% and 18.9 % in **1** and **2**, respectively. The 2D fingerprint plots are illustrated in **Figure 5b-d** and **5f-h** for compounds **1** and **2**, respectively.

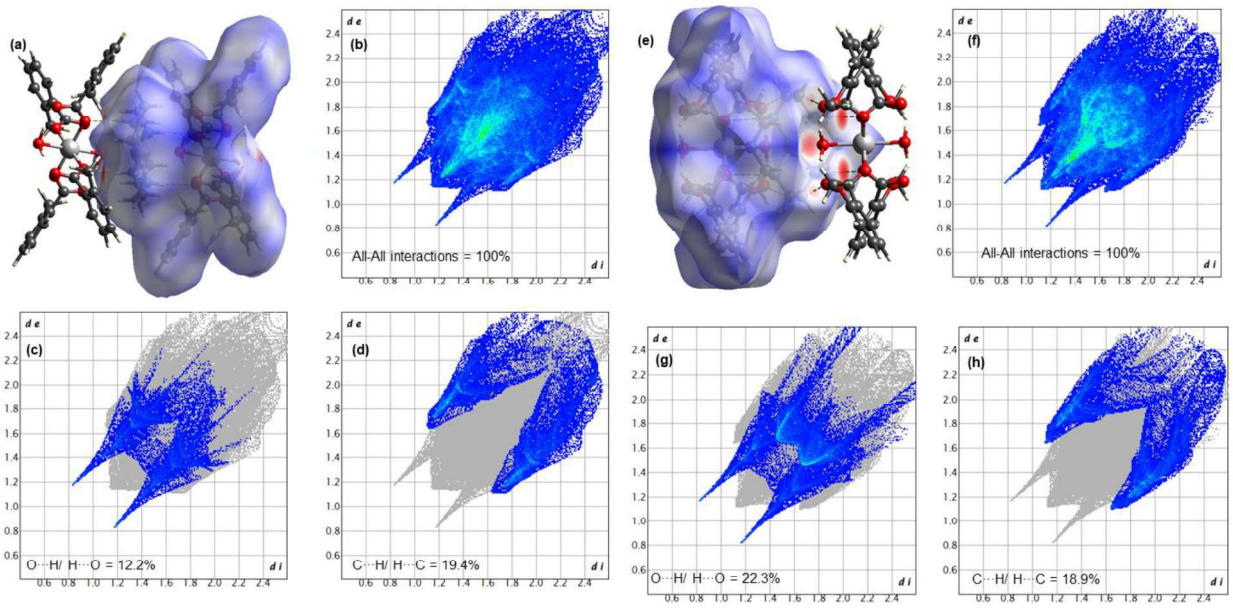

Figure 5 Intermolecular N-H···O interactions in **1 (a)** and **2 (e)**. 2D Fingerprint showing full, O···H/H···O and C···H/H···C type interactions with the percentage of contribution to the total Hirshfeld surface area in compound **1 (b-d)** and **2(f-h)**.

Interestingly, the 1-D chain structure in compound **2** was retained by substituting the methyl group with the methoxy group. This observation prompted further investigation with other simple substituents. Compound **3** was synthesized using the *o*-hydroxy benzoic acid. Structural analysis revealed that **3** formed a discrete zero-dimensional compound rather than a one-dimensional polymeric structure. Compound **3** crystallized in an orthorhombic crystal system with *P b c a* space group. The crystal structures consist of a unique zinc ion on the inversion center, due to which half of the molecule is symmetry generated. The zinc ion adopts the octahedral geometry with four equatorial positions of the octahedron occupied by the nitrogen atoms of the cyclam ligand (N1, $N1^{i}$, N2, $N2^{i}$). The axial positions are taken by the oxygen atoms (O1 and $O1^{i}$) contributed by the corresponding carboxylate anion, coordinating with the central metal ion *via* monodentate coordination mode shown in **Figure 6a**. Compound **3** is isomorphous to **4**, synthesized using o-nitrobenzoic acid. **4** exhibited similar unit cell parameters and coordination environment, as seen in **3**, depicted in **Figure 6b**. The distortion in the octahedron of **3** is evident from the slightly longer Zn-O (2.1874 (12) Å) bonds as compared to the Zn-N (2.0924 (14) Å) bond lengths. Similar observations are made for **4**. The selected bond lengths and angles of compound **3** and **4** are summarized in **Table S2**. The crystal packing is stabilized by non-covalent N-H···O, O-H···O, and C-H···O hydrogen bonds. The intermolecular bonding situation in **3,** wherein C9 (donor atom) of the cyclam ligand interacts with the adjacent molecules through the uncoordinated oxygen atom O2 (acceptor atom) with a D···A distance of 3.325 Å, as a result of which a supramolecular network is formed. A view of the supramolecular assembly of **3** is shown in **Figure 7b.** The hydrogen bonding parameters are summarized in **Table 3**.

a)

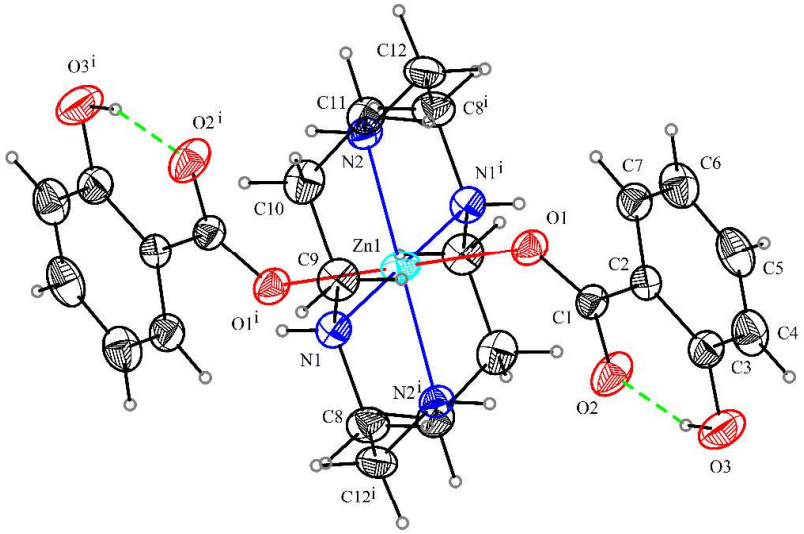

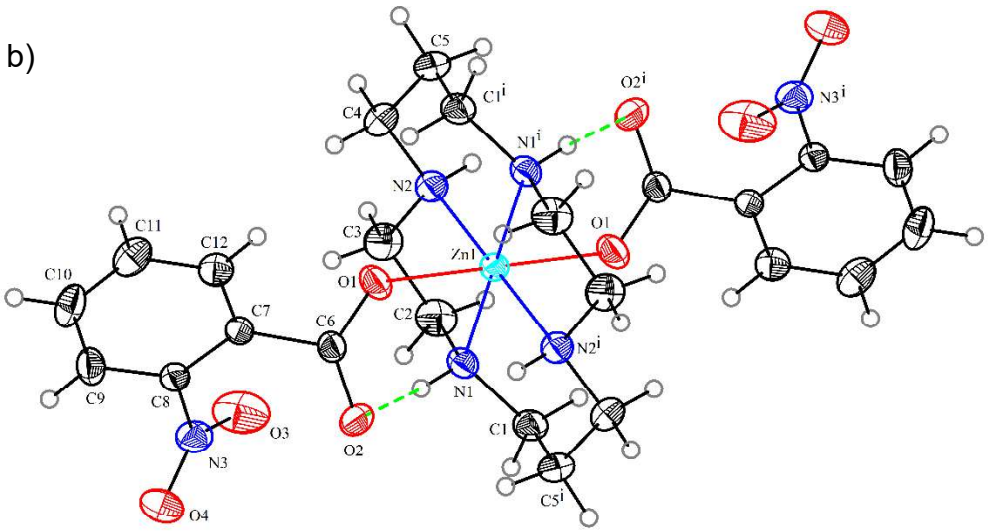

Figure 6. The thermal ellipsoid pot of compounds **3 (a)** and **4 (b)** with atom labeling scheme.

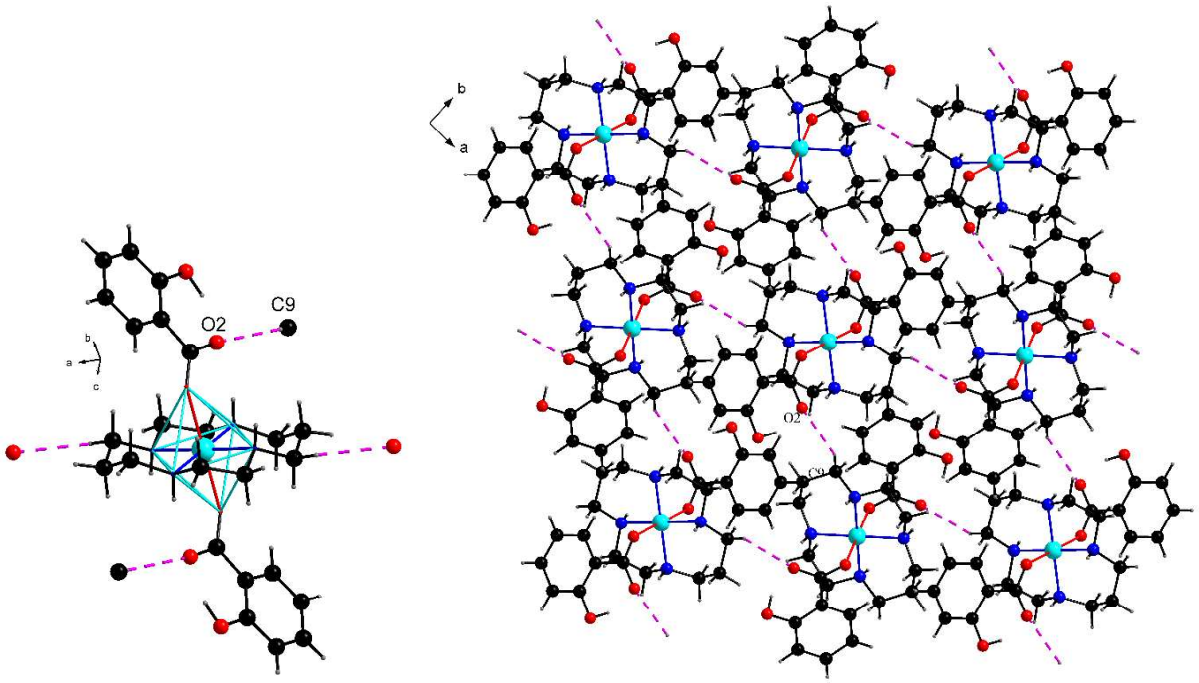

Figure 7 a) The C-H···O intermolecular hydrogen bonding situation in **3 b)** A view of 2D supramolecular network in **3.**

Compounds **3** and **4** showed isomorphism, reflected in the cell similarity index (π) with a value of 0.0192, which is very close to zero, suggesting a higher resemblance in the unit cell parameters. However, these two compounds do not exhibit isostructurality. The asymmetric units were further

overlaid to obtain the rmsD and max D values, as **Figure S4** depicts. A higher deviation of the max D value of 3.5487 indicates a variation in the crystal structure packing of the two compounds influenced by the different substituents. Unlike the methyl or methoxy substituent, the hydroxy substituent is involved in intramolecular hydrogen bonding with the carboxylate group through the uncoordinated oxygen atom (O2), which does not allow the carboxylate group to bend to a greater extent. The dihedral angle between the aromatic ring (C2-C3-C4-C5-C6-C7) carrying the substituent and the plane defined by (O1-C1-O2) is 10° in (**1**). On the contrary, the dihedral angle observed in **4** is 44.25 between the plane defined by (C7-C8-C9-C10-C11-C12) and (O1-C6-O2) shown in **Figure 8**. This variation could be one of the factors in disrupting the isostructurality between the two isomorphous compounds.

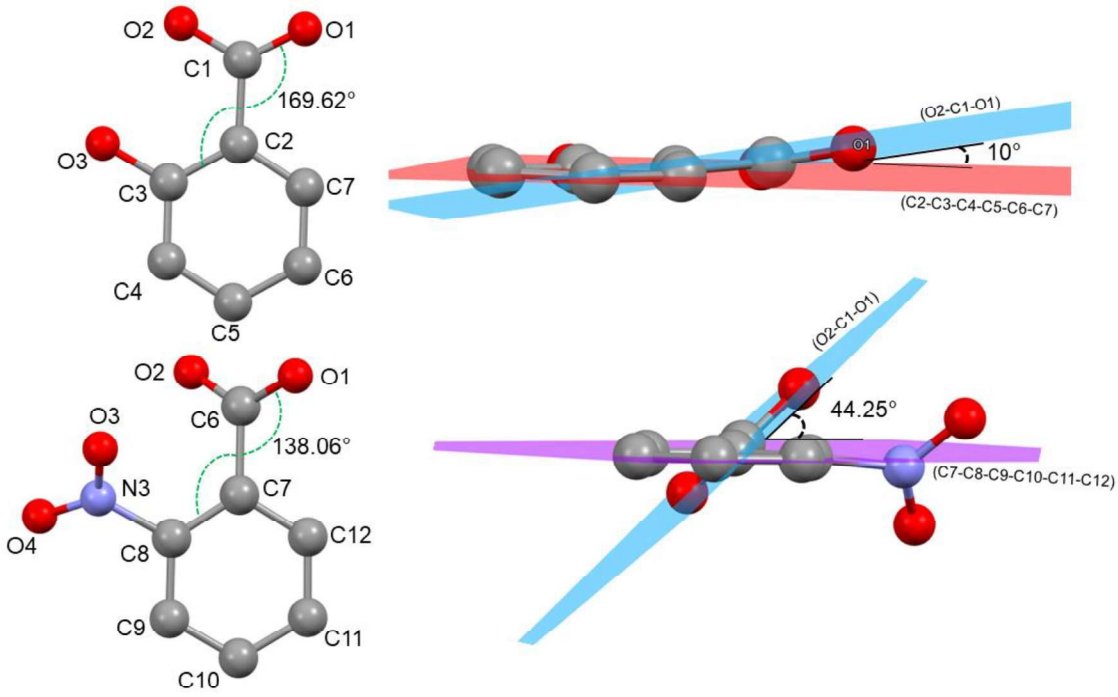

Figure 8 View along the carboxylate anion in **3** and **4** highlighting the orientation of the substituents (left) and dihedral angle between the mean plane through the benzene ring (C2-C3-C4-C5-C6-C7) and (O2-C1-O1) (**3**) and (C7-C8-C9-C10-C11-C12) and (O2-C6-O1) (right)

Additionally, we conducted Hirshfeld surface analysis on the two isomorphous compounds to gain insights into the supramolecular non-covalent interactions. The HS for **3** and **4** is mapped over the d_{norm} range (-0.1753 to 1.7791) and (-0.2183 to 1.3441), respectively. The d_{norm} surfaces are indicative of short contacts such as N-H···C formed between the cyclam ligand and the carbon

atom of the carboxylate ligand of neighboring molecule seen as a bright red area in the Hirshfeld surfaces (**Figure 9 a**). In the case of **4**, short contacts C-H···O are observed between the carbon atoms of the coordinated carboxylate (**Figure 9 b**), the oxygen atoms of the nitro group, and the uncoordinated oxygen atom of the carboxylate group. Comparatively, more O···H/H···O type interactions are witnessed in **4** with 32.2 % than in **3**, as depicted in the 2D figure print plot of **3** (**c** and **d**) and **4** in (**e** and **f**). The difference in the interaction between the adjacent molecules indicates different packing of the molecules in the crystal lattice, resulting in disruption in isostructurality.

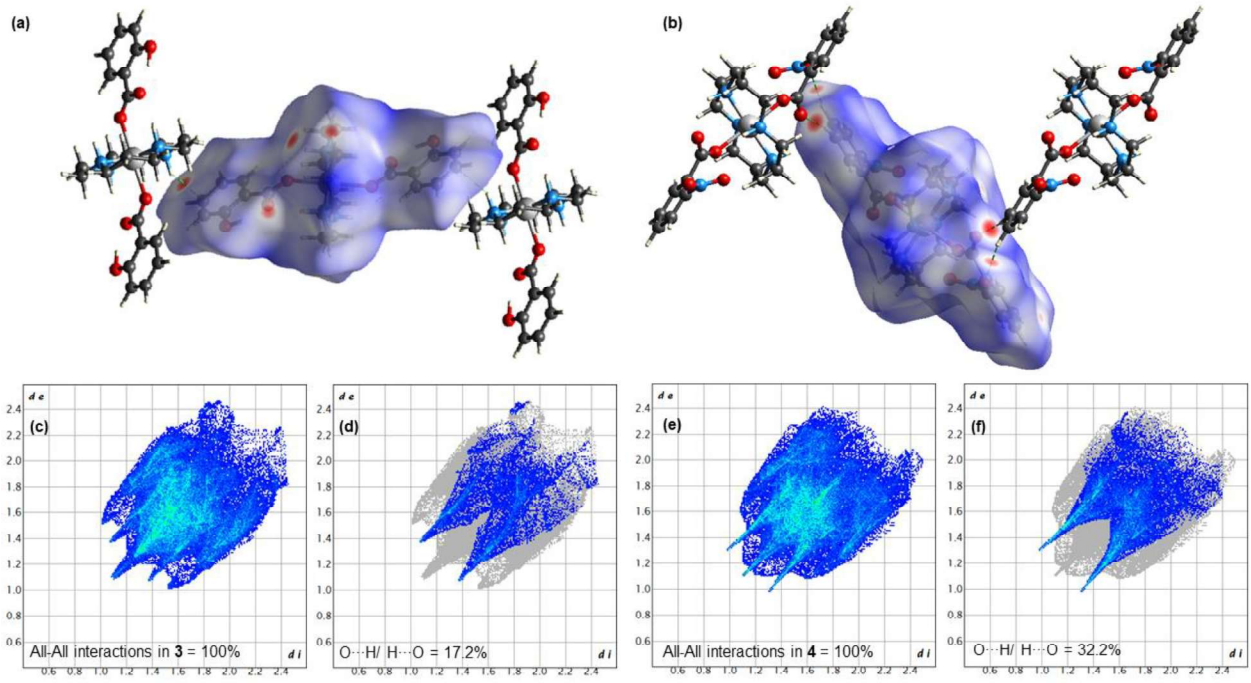

Figure 9 Intermolecular N-H···C interactions in **3 (a)** and C-H···O in **4 (b)**. 2D Fingerprint showing full and O···H/H···O type interactions with the percentage of contribution to the total Hirshfeld surface area in **3** and **4**.

Compounds **5-8** were synthesized using benzoic acid as the parent acid and other substituted benzoic acids with chloro, methyl(thio), and amino group at the ortho position. The crystal structure analysis revealed that, except for **8**, others showed isomorphism with similar unit cell parameters. Compounds **5-7** crystallize in a monoclinic crystal system with the $P2_1/n$ space group, while **8** crystallize in the $C2/c$ space group. All these compounds **5-8** have zinc ions placed in a special position. The asymmetric unit of compound **5** contains a Zn(II) ion coordinated to the cyclam ligand on the equatorial positions via the nitrogen atoms (N1, N2, N1i, and N2i) where *i*=

-x, 1-y, 1-z. In contrast, the axial positions are occupied by the oxygen atoms from the coordinated aqua molecules, forming a [ZnN4O2] coordination environment. The bond length of the metal to nitrogen of the cyclam Zn1-N1 = 2.1047 (10) Å, slightly shorter than the metal to the oxygen atom of the coordinated aqua ligand Zn-O bond distance is 2.2453(10) Å. Similar observations are made for compounds **6**, **7**, and **8**. The selected bond angles and bond distances are summarized in **Table S2**. These bond distances and angles are consistent with the similarly reported compound having $[Zn(cyclam)]^{2+}$ cationic core[27-30]. This cationic unit then interacts with the uncoordinated carboxylate anions through intramolecular hydrogen bonds, arising from the O-H of the aqua molecules with the uncoordinated oxygen atom of the carboxylate group acting as the hydrogen bond acceptor atoms and resulting in the formation of a zero-dimensional mononuclear compound. Compound **7** differs slightly from their isomorphous group (**5** and **6).** It contains four aqua molecules in its crystal lattice, which results in additional hydrogen bonding. The crystal structure of compounds **5** and **7** are shown in **Figure 10**, while the figures for compounds **6** and **8** are in the supplementary information (**Figure S5**).

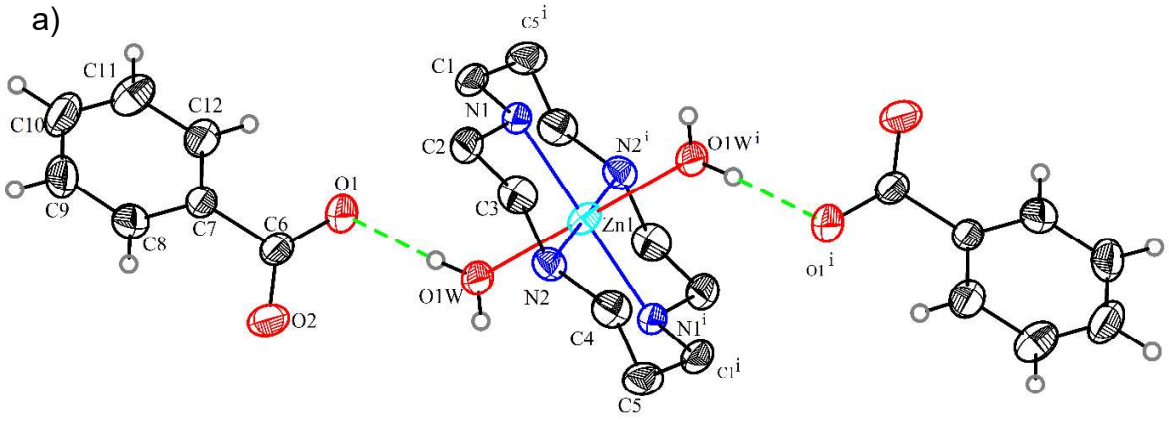

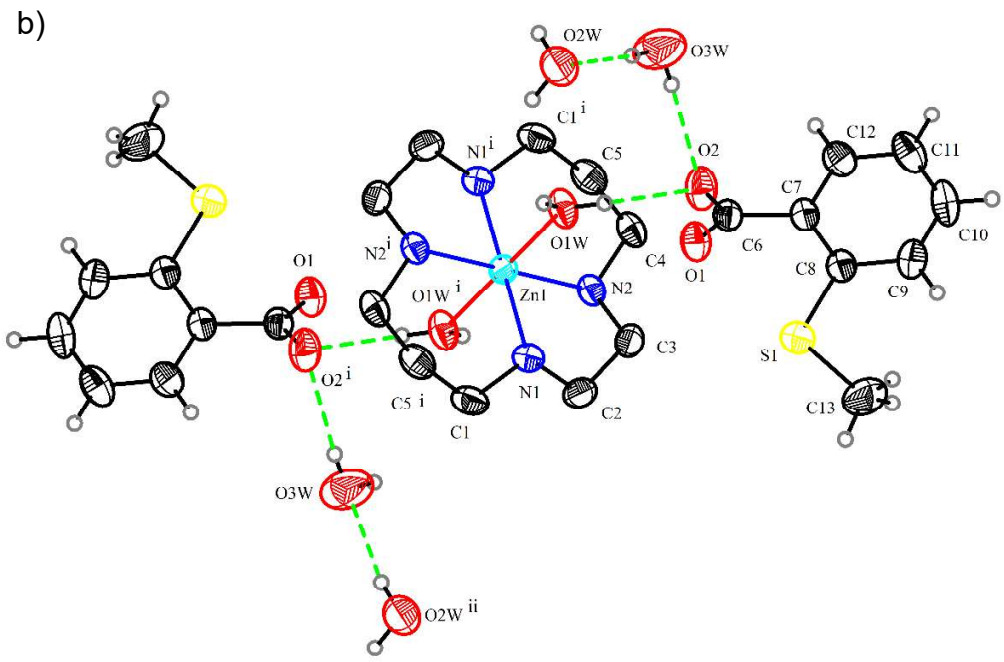

Figure 10. The thermal ellipsoid pot of compounds **5 (a)** and **7 (b)** with atom labeling scheme.

Several non-covalent interactions attain the crystal packing in the isomorphous compounds 5-7, majorly of the type O-H···O, N-H···O and C-H···O hydrogen bonds interactions (**Table 3**). Compounds **5** and **6** both exhibit a total of four hydrogen bonds, among which two are intermolecular N-H···O and O-H···O type hydrogen bonds responsible for the extension of the discrete unit in a one-dimensional supramolecular chain along the axes depicted in **Figure 11a**. It can be further seen that the ligated aqua molecules are involved in hydrogen bonding with the oxygen of the carboxylate group O1W-H1W···$O1_{(intra)}$ and O1W-H2W···$O2_{(inter)}$, resulting in the formation of edge-fused R_2^2 (8) ring along the ***ac*** plane with H···*A* distances of 1.887 and 1,980 Å, accompanied by the *D*-H···*A* of 176.47 and 159.77º respectively in **5**. A similar arrangement was observed in compound **6**. On the other hand, compound **7** exhibits more hydrogen bonding interaction due to non-ligated water molecules in its structure. Compound **7** exhibits eleven hydrogen bonds, four intramolecular and seven intermolecular hydrogen bonds. The cationic unit interacts with the charge-balancing carboxylate anion via intramolecular hydrogen bond interaction (O1W-H2C···O2), where O1W atoms act as the donor and O2 acts as the acceptor atoms with H···*A* distance of 1.923 Å. The other hydrogen of the O1W is involved in interlinking the adjacent units via (O1W-H1C···$O1^{ii}$) interaction, where (*ii = (1-x, 1-y, 1-z*), thus forming a similar eight-membered ring structure as seen in **5** and **6** resulting in one-dimension

supramolecular chain structure along the **b** axes (**Figure 11 b**). The non-ligated ligand aids in interlinking the individual chain structure by forming a four-membered water cluster, which extends along the ac plane, thereby rendering a 2D layered supramolecular network in compound **7**, as depicted in the supplementary information (**Figure S6**). These structural changes indicate little or no isostructurality between **5**, **6**, and **7**.

A view of the supramolecular assembly of compound **8** is exhibited in **Figure 12**, The crystal packing here is stabilized mainly by N-H···O and O-H···O type of interactions (**Table 3**) with H···O distance in the range of 2.041 to 2.611 Å. compound **8** exhibits two intra- and four intermolecular hydrogen bonding interactions responsible for stabilizing the crystal structure. The amino group, unlike other substituents, participates in hydrogen bonding with the unbounded carboxylate oxygen (O2), resulting in the formation of a chain-like structure, interlinking the cationic units, thus resulting in the formation of a 1D ladder-shaped supramolecular layer.

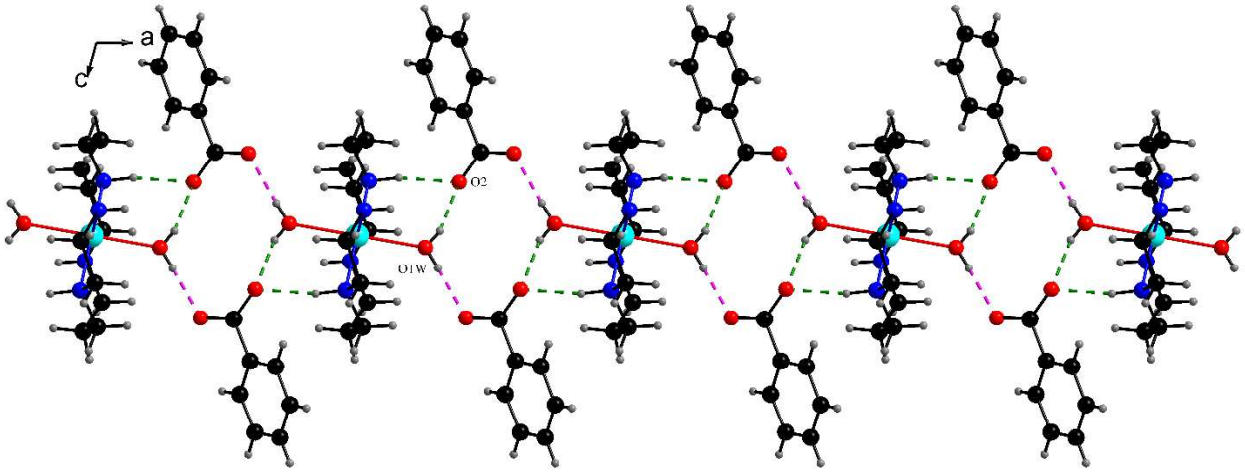

Figure 11a. Formation of 1D supramolecular chain through N1-H1···O2 and O1W-H···O2 shown in purple dotted lines in **5**.

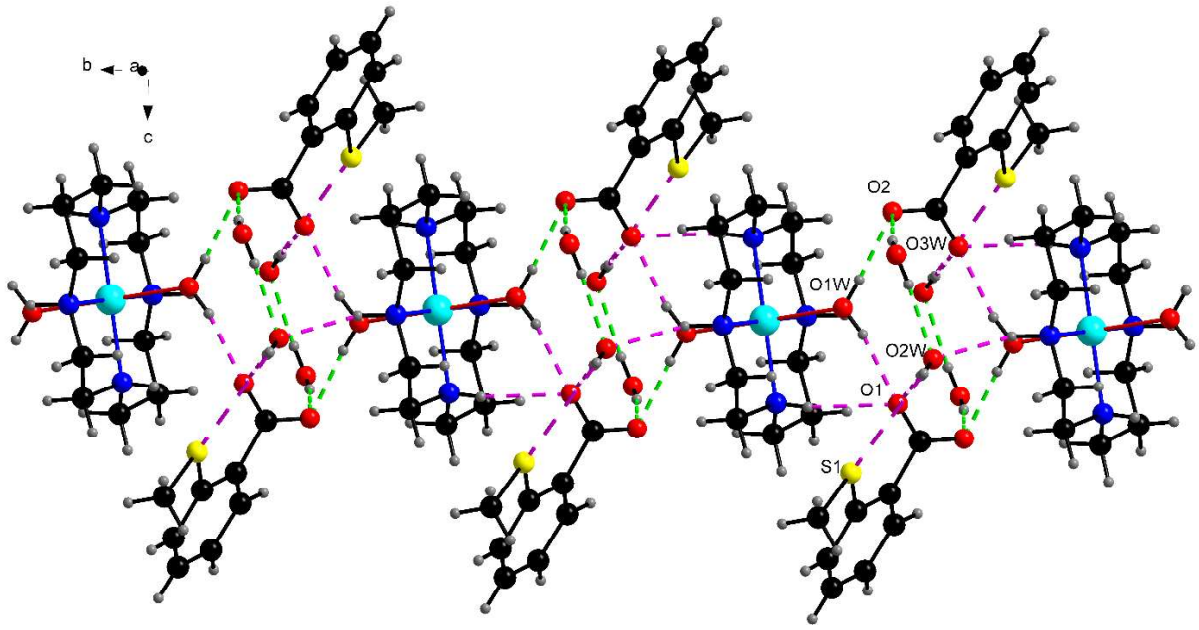

Figure 11 b. Formation of 1D supramolecular chain structure via N-H···O, O-H···O and O-H···S type of intermolecular interactions shown in purple dotted lines in **7**.

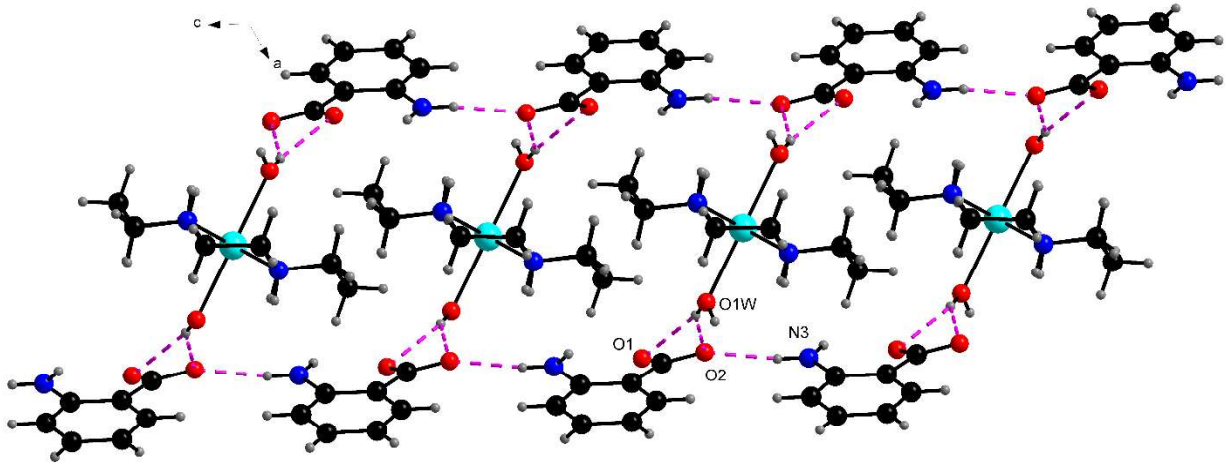

Figure 12. Formation of 1D supramolecular double chain structure via N-H···O and O-H···O interactions shown in purple dotted lines in **8**.

It is evident that compounds **5**-**7** lack isostructurality due to significant variations in the hydrogen bonding situation in the crystal structure upon including different substituents. The cell similarity index π value for the molecular pair **5**/**6** is 0.0197, whereas, for **5**/**7**, it increases up to 0.2452. The highest deviation of the cell similarity index from zero is seen in the case of a **5**/**7** pair. It is attributed to the intense hydrogen bonding situation in compound **7**, which comprises non-ligated water molecules.

The Hirshfeld surface is mapped over d_{norm} range (-0.7068 to 1.4553) in **5**, (-0.72 to 1.3264) in **6** and (-0.6574 to 1.6115) in **7**. The red spots on the surface indicate the dominant interactions. The HS analysis indicates strong hydrogen bond interactions such as O-H···O and N-H···O co-exist between the cationic and the anionic unit in **5**-**7** shown in (**Figure 13 a-c**), respectively. The 2D fingerprint plots **5** -**7** shown in the supplementary information (**Figure S7**) exhibit the crucial contributors to crystal packing; the results are also expressed as a pie chart in **Figure 13 d-f** for compounds **5**-**7**. The majority of the contribution in all isomorphous compounds arises from the H···H type in the order of **5** > **7** > **6**. Compared to the parent compound (**5**), **6** and **7** exhibits H···Cl with 13.4 % contribution and H···S type with 6.7 % contribution in the respective compounds. Consequently, the additional interactions seen in **6** and **7** alter the crystal packing, thereby preventing the attainment of isostructurality.

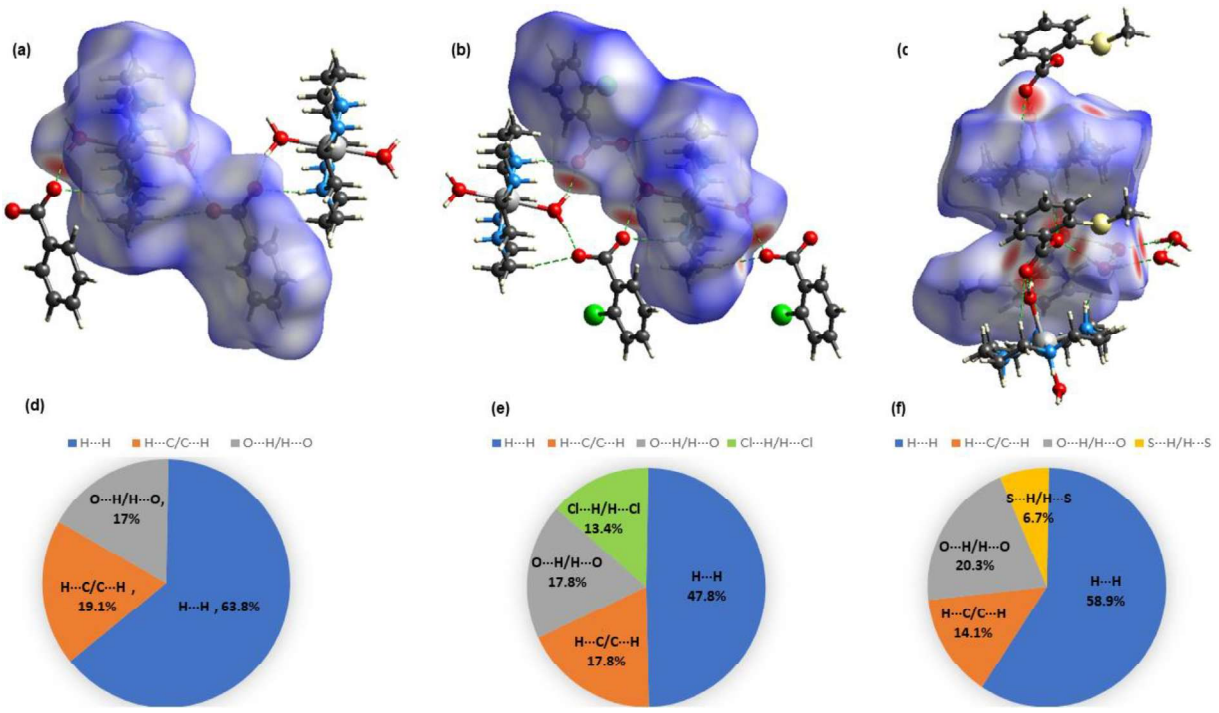

Figure 13 Intermolecular O-H···O and N-H···O type non-covalent interactions in **5** (a), **6**(b) and **7**(c).

2. 4. X-ray Powder diffraction

We then recorded their powder X-ray diffraction patterns to investigate the phase purity of the bulk material. The stimulated data for all the compounds were obtained from the Mercury 4.0 software. The diffractograms for compounds **1** and **2** are shown in **Figure 14**, whereas for compounds 3/4 and 5-8, the powder patterns are given in **Figures S8** and **S9**, respectively. The diffraction peaks in the stimulated pattern exactly matched the experimental data collected at room temperature, suggesting that the single crystal model represents the bulk crystalline material. Powder diffractograms can be a suitable technique for identifying isostructurality in related compounds as they show unique fingerprints of the solid compounds. Upon comparing the powder patterns of the related compounds, such as **1** with **2**, **3** with **4**, and **5**-**7**, it was observed that the powder patterns slightly varied, again suggesting that the related compounds sharing similar unit cell parameters are not isostructural.

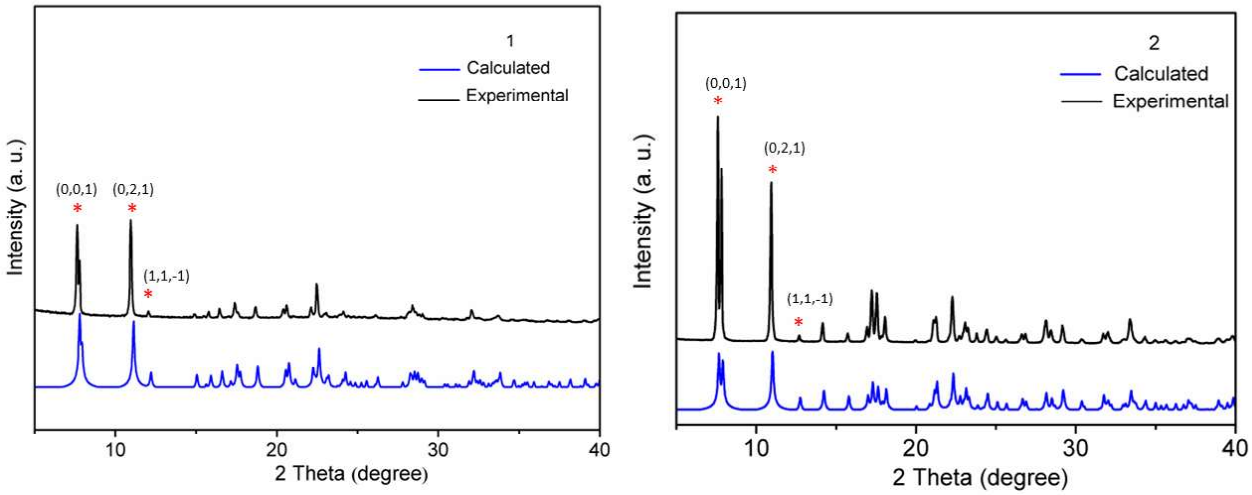

Figure 14 The XRD powder patterns of **1** and **2**

3. Conclusion

Eight zinc compounds (**1**-**8**) were synthesized and characterized using analytical techniques. The structural analysis of these compounds led to the exploration of rich solid-state chemistry, specifically dealing with the interaction of the carboxylate ligand with the zinc cyclam unit. The structural variation was achieved by switching the substituents at the *ortho* position relative to the carboxylate group on the aromatic ring. Introducing the methyl and methoxy substituents (**1**) and (**2**), respectively, resulted in a one-dimensional coordination polymer. In the structure, aqua molecules bridged the zinc ions of the cationic and the anionic units. The thermal profile of **1** was compared with **5**; it was observed that in **1**, the dehydration step appeared at a much higher temperature range than the dehydration in compound **5,** this is attributed to the different modes of coordination adopted by the aqua molecules in **1** and **5.** Compounds **1** and **2** further shared similar unit cell parameters with cell similarity index values close to zero; thus, the ISOS software identified the two compounds as isomorphous. However, a lower isostructurality index and larger deviation in the Dmax value obtained by overlaying the asymmetric units of **1** and **2** in mercury software suggested that the related compounds, although they share similar unit cell parameters, were not isostructural. The loss in isostructurality is attributed to the preference of the non-covalent interactions and orientation of the substituents relative to the coordinating carboxylate group in the

respective compounds. These non-covalent interactions are theoretically predicted by Hirshfeld surface analysis. Similarly, compound **3** was isomorphous to **4**; here, the carboxylate ligand coordinated directly with the zinc ions, rendering a zero-dimensional compound. In **5**-**8**, the carboxylate ligands did not coordinate with the zinc ion. They were held by the intramolecular hydrogen bonds in the crystal lattice, with compound **7** also exhibiting additional aqua molecules in the crystal lattice. The compounds **5**-7 showed isomorphism, with significant variation in the packing arrangement because of the chloro and (methylthio) substituents in the lattice compared to the parent benzoate ligand. The addition of these substituents breaks the isostructurality as they introduce the additional Cl···H/ H···Cl and S···H/ H···S type of non-covalent interactions as identified theoretically by Hirsfeld surface analysis.

Author Contribution:

Nikita N. Harmalkar: Investigation, methodology, data curation, formal analysis, conceptualization, visualization, writing original draft, writing -review & editing.

Sunder N. Dhuri: Methodology, conceptualization, writing original draft, writing -review & editing, project administration, funding acquisition, supervision, visualization, validation.

Conflicts of interest

There are no conflicts of interest to declare.

Supplementary information (SI)

Additional crystallographic information can be found in the joint Cambridge Crystallographic Data Centre (CCDC) and is available without charge: the deposition numbers CCDC 2376524 (**1**), 2376525 (**2**) 2376526 (**3**), 2376527 (**4**), 2376528 (**5**), 2376529(**6**), 2376530 (**7**) and 2376531 (**8**). Supplementary Data (Fig. S1 and S9) and (Tables S1 and S2) associated with this article are electronic.

Acknowledgments

The authors thank the Department of Science and Technology (DST), New Delhi, India, for DST-FIST (SR/FST/CSII-034/2014(C) project and the University Grants Commission (UGC), New Delhi, India, for the UGC-SAP (F.504/14/DSA-I/2015) project. SND thanks the Council of

Scientific and Industrial Research (CSIR), New Delhi, India (No. 01(2923)/18/EMR-II) for financial support. SND thanks the Goa State Research Foundation (GSRF/Schemes/MajorGR /13/2023/187/ii) for its research support. NNH acknowledges UGC for providing her financial support under the Savitribai Jyotirao Phule Fellowship for Single Girl Child (SJSGC) [UGCES-22-OB-GOA-F-SJSGC-6907].

References

[1] N. AlHaddad, E. Lelong, J.-M. Suh, M. Cordier, M. H. Lim, G. Royal, C. Platas-Iglesias, H. Bernard, R. Tripier, *Dalton Trans*., 2022, **51**, 8640.

[2] L. M. P. Lima, Z. Halime, R. Marion, N. Camus, R. Delgado, C. Platas-Iglesias, R. Tripier, *Inorg. Chem.*, 2014, **53**, 5269–5279.

[3] X. Liang, P. J. Sadler, *Chem. Soc. Rev.,* 2004, **33**, 246-266.

[4] T. Chen, X. Wang, Y. He, C. Zhang, Z. Wu, K. Liao, J. Wang, Z. Guo, *Inorg. Chem*. 2009, **48**, 5801–5809.

[5] R. Reichenbach-Klinke, B. König, *J. Chem. Soc., Dalton Trans*., 2002, 121-130.

[6] P. Mahato, A. Ghosh, S. K. Mishra, A. Shrivastav, S. Mishra, A. Das, *Inorg. Chem*. 2011, **50**, 4162–4170.

[7] B. Bosnich, C. K. Poon, M. L. Tobe, *Inorg. Chem*. 1965, **4**, 1102–1108.

[8] T. M. Hunter, S. J. Paisey, H.-S. Park, L. Cleghorn, A. Parkin, S. Parsons, P. J. Sadler, *J. Inorg. Biochem.*, 2004, **98**, 713-719

[9] L. G. Alves, M. Souto, F. Madeira, P. Adão, R. F. Munhá, A. M. Martins, *J. Organometallic Chem*., 2014, **760**, 130-137

[10] T. M. Hunter, I. W. McNae, D. P. Simpson, A. M. Smith, S. Moggach, F. White, M. D. Walkinshaw, S. Parsons, P. J. Sadler, *Chem. Eur. J*., 2007, **13**, 40-50

[11] S. O. Alzahrani, G. McRobbie, A. Khan, T. D'huys, T. Van Loy, A. N. Walker, I. Renard, T. J. Hubin, D. Schols, B. P. Burkea, S. J. Archibald, *Dalton Trans*., 2024, **53**, 5616-5623

[12] N. AlHaddad, E. Lelong, J.-M. Suh, M. Cordier, M. H. Lim, G. Royal, C. Platas-Iglesias, H. Bernard, R. Tripier, *Dalton Trans*., 2022, **51**, 8640-8656.

[13] N. N. Harmalkar, S. Gaonkar, D. A. Barretto, S. N. Dhuri, *Inorg. Chim. Acta*, 2024, **569**, 122139

[14] X. Liang, M. Weishäupl, J. A. Parkinson, S. Parsons, P. A. McGregor, P. J. Sadler, *Chem. Eur. J.* 2003, **9**, 4709–4717.

[15] A. Ross, J.-H. Choi, T. M. Hunter, C. Pannecouque, S. A. Moggach, S. Parsons, E. De Clercq, P. J. Sadler, *Dalton Trans*., 2012, **41**, 6408-6418

[16] H. Jo, A. J. Lough, J. C. Kim, *Inorganica Chim. Acta,* 2005, **358**, 1274-1278.

[17] J. Chang Kim, A. J. Lough, H. Park, Y. C. Kang, *Inorg. Chem. Commun*. 2006, **9**, 514-517.

[18] P. Bombicz, N. V. May, D. Fegyverneki, A. Saranchimeg, L. Bereczki, *CrystEngComm*, 2020, **22**, 7193-7203.

[19] P. Bombicz, IUCrJ, 2024, 11, 3-6

[20] D. Dey, D. Chopra, *Cryst. Growth Des*. 2017, **17**, 5117–5128

[21] M. Indrani, R. Ramasubramanian, F. R. Fronczek, N. Y. Vasanthacharya, S. Kumaresan, *J. Mol. Struct.* 2009, **931**, 35-44

[22] J. Cao, Y. Gao, Y. Wang, C. Du, Z. Liu, *Chem. Commun*., 2013, **49**, 6897-6899.

[23] S. Mukherjee, S. Ganguly, K. Manna, S. Mondal, S. Mahapatra, D. Das, *Inorg. Chem*. 2018, **57**, 4050-4060.

[24] K. U. Narvekar, B. R. Srinivasan, *Acta Cryst*., 2020, **E76**, 1260-1265.

[25] S. Kumar, R. P. Sharma, A. Saini, P. Venugopalan, V. Ferretti, *J. Mol. Struct.* 2015, **1083**, 398-404.

[26] H. Pérez, A. Di Santo, O. E. Piro, G. A. Echeverría, M. González, A. B. Altabef, R. M.Gomila, A. Frontera, *Dalton Trans*., 2021, **50**, 17029-17040.

[27] N. W. Alcock, A. Berry, P. Moore, *Acta Cryst*., 1992, **C48**, 16-19.

[28] R. I. Gurtovyi, S. P. Gavrish, L. V. Tsymbal, M.-O. Apostu, M. Cazacu, S. Shova, Y. D. Lampeka, *Polyhedron*, 2022, **221**, 115870-115882.

[29] L. V. Tsymbal, I. L. Andriichuk, V. Lozan, S. Shovac, Y. D. Lampeka, *Acta Cryst*., 2022, **E78**, 625-628.

[30] S.-L. Huang, L. Zhang, Y.-J. Lin, G.-X. Jin, *CrystEngComm*., 2013, **15**, 78-85.

Click here to access/download

Supporting Information

Zinc_SI_SND_NNH.docx